Multi-Object Bayesian Filters with Amplitude Information in Clutter Background

Bin Yang[a,*], Jun Wang[a], Changshun Yuan[a], J. Thiyagalingam[b], T. Kirubarajan[c]

[a] *School of Electronic and Information Engineering, Beihang University, Beijing, China*
[b] *Department of Electrical Engineering and Electronics, University of Liverpool, Liverpool, United Kingdom*
[c] *Electrical and Computer Engineering Department, McMaster University, Hamilton, Ontario, Canada*

Abstract

In many radar or sonar tracking applications, the amplitude information (AI) is known to improve data association and target state estimation in most of multi-object filters. However, when considering targets in noisy backgrounds, existing multi-object filters rely on a number of assumptions, relating to the uniformity of the spatial distribution of the clutter and amplitude distribution of the clutter being Rayleigh. These assumptions are seldom held under realistic conditions, and as such, the underlying multi-object filters deliver a sub-optimal tracking performance. In this paper, we incorporate the AI as part of the multi-object filtering process to render very novel filters that can handle multi-object tracking in much more difficult and realistic conditions. In particular, we propose an inverse Gamma Gaussian Model for the target and clutter state, consisting of kinematic state and return power. We then develop the inverse Gamma Gaussian Mixture (IGGM) implementation of the RFS filters with AI. Simulations show that proposed filters, in particular when combined with clutter estimation and its RFS approximation, are more robust in handling a number of realistic cases when compared against existing filters.

*Corresponding author.
Email addresses: young.being1990@gmail.com;young_being@buaa.edu.cn (Bin Yang), wangj203@buaa.edu.cn (Jun Wang), yuanchang61@buaa.edu.cn (Changshun Yuan), tjeyan@liverpool.ac.uk (J. Thiyagalingam), kiruba@mcmaster.ca (T. Kirubarajan)

Keywords: Multi-object tracking, amplitude information, clutter estimation, random finite sets, PHD filter, CPHD filter, CBMeMBer filter

1. Introduction

1.1. Background and Motivation

In the context of multi-target tracking, multi-object filters jointly estimate the number of targets and their states from a history of measurements. However, the performance of these filters deteriorate very rapidly due to a number of reasons such as missed detections from non-ideal sensors, false alarms arising from non-target originating returns, and incorrect measurement-to-target associations. On this note, by complementing the existing multi-target tracking algorithms, such as joint probabilistic data association (JPDA) filter, multiple hypothesis tracking (MHT) algorithm, and random finite set (RFS)-based filters, and by incorporating the amplitude (or signal strength) information (AI), it is possible to improve the estimation performance. This is becoming increasingly feasible with modern sensors where the outputs include AI along with the conventional kinematic measurements.

Using AI as part of the multi-target tracking has been explored before. For instance, in [1], AI is used to enhance the data association of the probabilistic data association (PDA) algorithm. In [2] and [3], AI is used to enhance the MHT algorithm. In [4], target amplitude strength is introduced into a closely-spaced target tracking model for improving the tracking performance. In [5], the target amplitude feature is modeled as a Rayleigh likelihood function of the target mean signal-to-noise ratio (SNR), and is incorporated into the probability hypothesis density (PHD) and cardinalized PHD (CPHD) filters. In [6], a cardinality-balanced multi-target multi-Bernoulli (CBMeMBer) filter with AI is proposed. In [7], a more robust multi-object, multi-Bernoulli filter incorporating AI (MeMBer-AI) is proposed to handle unknown clutter rate. In [8, 9, 10], the AI is used in conjunction with multi-object filtering for estimating the target states and their radar cross sections (RCSs) for robust ground target tracking using airborne radar measurements. However, the direct utility of these approaches is based on one or more assumptions, including: a) spatial density of the clutter being uniform; b) clutter amplitude being Rayleigh-distributed; and c) the clutter model is known *a priori*.

In practice, however, these assumptions rarely hold true. For instance, when tracking a faint target over a ground- or sea- background, the AI is often same as the background information, and thus they are non-distinguishable. Similarly, spatial density of the clutter and/or the distribution of the clutter amplitude may often be non-uniform and/or non-Rayleigh, for instance when considered over a heterogeneous terrain. As such, it is difficult to treat clutter models as known *a priori*, which often leads to sub-optimal tracking performance.

1.2. Brief Survey of Related Work

A number of approaches for estimating the parameters of clutter models in the context of multi-object filtering have been proposed before. For instance, conventional approaches, such as [11], estimate the parameters that characterize the clutter model independent of the filtering. In [12] and [13], based on Poisson clutter process assumption, a generalization of the PHD filter, called the intensity filter, augments the target state space with clutter state space, which can estimate the clutter model while filtering. Approaches for jointly estimating the clutter and kinematic states in an unknown clutter background are proposed in [14] and [15]. The approaches, κ-PHD and κ-CPHD filters, perform this by relying on a Bernoulli clutter generator. A Bernoulli clutter generator is, like a target, a Bernoulli RFS. It generates at most a single observation at a time and has an unknown state. According to a Markov motion model, the state of the clutter generator is propagated with time. The total clutter process is modeled as the union of an unknown number of Bernoulli clutter generators. The number and states of the targets can be estimated simultaneously with the number and states of the clutter. Mahler *et al.* implemented the κ-PHD and the κ-CPHD filters by using a Beta-Gaussian Mixture (BGM) approximation. Under BGM approximation, the intensity function of the clutter can be estimated in closed-form as a Gaussian mixture. Another implementations of the κ-PHD and the κ-CPHD filters are proposed in [16] and [17], respectively, which approximate the intensity function of the clutter by using a Normal-Wishart mixture (NWM). The robust CBMeMBer filter is proposed in [18] and its applicabilities were demonstrated using two examples on visual tracking [19] and sensor management [20, 21].

Although the literature presented above provides a suite of powerful techniques and methods to relax the assumptions relating to the model of the clutter, the key limitation is that all these considered only the spatial distribution of clutter. As such, they are not directly applicable towards relaxing any assumptions on the amplitude distribution of clutter. To the best of our knowledge, our study here is the first one to make such an approach. Utilizing the AI as part of the joint estimation of target states and parameters of the clutter model, is likely to lead to better outputs, and thus improved multi-object tracking performance. In this paper, we use the AI to improve the performance of multi-object filters in a clutter environment, with a special focus on relaxing the assumptions outlined above.

In performing the proposed study, this paper makes the following contributions:

- By modeling the amplitude features of the target and the clutter using different distributions, namely the Rayleigh and the Weibull, which is often adopted in the context of the GMTI radar or sea radar, we simultaneously incorporate the AI into the target state filtering and clutter estimation steps;

- To incorporate the AI into the existing clutter-agnostic multi-object filter algorithms, such as the κ-PHD, κ-CPHD and the robust CBMeMBer filters, we propose an inverse Gamma Gaussian (IGG) model with an augmented state, consisting of the kinematic state and the return power, which are assumed to be independent of each other. Then, we develop the IGG mixture implementation of these filters with the AI;

- Using a number of simulations mimicking realistic scenarios that relax a number of assumptions outlined above, we show that the our proposed AI-incorporated multi-object filters outperform the conventional filters, and offer superior multi-object tracking performance.

The rest of the paper is organized as follows. In Section 2, we present the essential background of the multi-object Bayesian filtering and demonstrate how the amplitude information can be introduced into the multi-object Bayesian filter and clutter estimation. In Section 3, we present the amplitude model in noise-only and clutter background. In Section 4, we derive the IGG model and the IGGM implementations of the PHD, CPHD, and the CBMeMBer filters with AI. We then evaluate the performance of our proposed approach in Section 5 using a number of simulated, yet realistic, scenarios. Finally, we conclude the paper in Section 6.

2. Multi-Object Bayesian Filter with Amplitude Information

2.1. Multi-Object Bayesian Filter

Robustly tracking objects in a multi-object tracking scenario is centered around three key aspects:

1. The ability to handle the variation of the number of objects with time, which is directly linked to objects appearing and disappearing within and off the region of detection;
2. The ability to handle observations coming from imperfect sensors that consists of missed and false detections, which is a collection of measurements that are not associated with the targets; *and*
3. The ability to handle association of observation-to-target, which is ambiguous when targets are closely spaced.

The aim of a multi-object Bayesian filter is to handle these three cases at the same time by jointly estimating the number of time-varying objects, and their states from accumulated observations.

To this end, let $N(k)$ and $M(k)$ be the number of targets and observations at time k, along with the fact that $x_{k,1}, \ldots, x_{k,N(k)} \in \mathcal{X}$ and $z_{k,1}, \ldots, z_{k,M(k)} \in \mathcal{Z}$, are the corresponding states and observations. Corresponding multi-object state and the multi-object observations are then represented by the following finite sets:

$$X_k = \left\{x_{k,1}, \ldots, x_{k,N(k)}\right\} \in \mathcal{F}(\mathcal{X}) \tag{1}$$

and

$$Z_k = \left\{z_{k,1}, \ldots, z_{k,M(k)}\right\} \in \mathcal{F}(\mathcal{Z}) \tag{2}$$

where $\mathcal{F}(\mathcal{X})$ and $\mathcal{F}(\mathcal{Z})$ are the finite subsets of $\mathcal{X}$ and $\mathcal{Z}$, respectively.

Using the random finite set formulations, the multi-object Bayesian recursion propagates the posterior probability density of a multi-object state $f_{k|k}(X_k|Z_{1:k})$ over time, according to

$$f_{k+1|k}(X|Z_{1:k}) = \int f_{k+1|k}(X|X')f_{k|k}(X'|Z_{1:k})\delta X' \tag{3}$$

$$f_{k+1|k+1}(X|Z_{1:k+1}) = \frac{f_{k+1|k}(Z_{k+1}|X)f_{k+1|k}(X|Z_{1:k})}{\int f_{k+1|k}(Z_{k+1}|X)f_{k+1|k}(X|Z_{1:k})\delta X} \tag{4}$$

where $Z_{1:k} = (Z_1, \ldots, Z_k)$ denotes the accumulated observations up to time k, $f_{k+1|k}(X|X')$ denotes the multi-object transition density, and $f_{k+1|k}(Z_{k+1}|X)$ denotes the multi-object likelihood. Here, the multi-object transition density accounts for the uncertainty on the number of targets while the multi-object likelihood accounts for the detection uncertainty.

With (3) and (4) involving multiple integrals on the space of $\mathcal{X}$, the optimal multi-object Bayesian filter cannot be implemented in a computationally tractable manner. This issue can, however, be addressed using a number of approximations, based on the idea of propagating moment or parameterized approximations, such as PHD, CPHD and CBMeMBer filters [22, 23, 24]. Instead of propagating the full multi-target density $f_{k|k}(X_k|Z_{1:k})$, the PHD and CPHD filters propagate their first-order moments, which are called PHDs, and cardinality distributions [22, 25]. The CBMeMBer filter approximates the multi-target density as multi-Bernoulli RFS, and thus propagates the set of multi-Bernoulli parameters. These multi-object filters have successfully been applied across a range of problems stemming from a number of domains, such as image processing, robotics and surveillance [26, 27, 28, 29].

In comparison to the fixed clutter models known *a priori*, clutter-agnostic models, which simultaneously estimate the target and clutter states, proven to be more effective [30]. In the following sub-sections, we outline how we intend to augment the capability of these robust filters by including the AI.

2.2. Amplitude Information Likelihoods

Let x^t denote the augmented state of a target that contains the kinematic state $\tilde{x}^t = [p_x^t, p_y^t, \dot{p_x^t}, \dot{p_y^t}]^T$, with p_x and p_y being the positions and $\dot{p_x}$ and $\dot{p_y}$ being corresponding velocities. Furthermore, let σ^t and σ^c be the power-linked attributes of the target and the clutter, respectively. In the context of radar signal processing, σ^t can either be the equivalent power of the receiver input, RCS or mean SNR, and σ^c can be the power of the clutter. In this paper, we define σ^t and σ^c as the target equivalent power and the clutter equivalent power of the receiver input, respectively. These are the powers of baseband signals after preprocessing, such as frequency conversion, amplifying and demodulation. With this definition, the augmented state x^t is defined as:

$$x^t := \begin{bmatrix} \tilde{x}^t \\ \sigma^t \end{bmatrix} \tag{5}$$

In addition to this, the state of clutter should also be considered when dealing with a clutter background. Similar to (5), the augmented clutter state x^c is defined as:

$$x^c := \begin{bmatrix} \tilde{x}^c \\ \sigma^c \end{bmatrix} \tag{6}$$

where $\tilde{x}^c = [p_x^c, p_y^c]^T$ represents the spatial state of clutter.

Considering the fact that the observation detected from the receiver consists of a two-dimensional target position $\tilde{z}$ and amplitude $a \geq 0$, the following assumption can be formulated.

Assumption 1. *The amplitude of the signal return is independent of state location, and the likelihoods for target $g^t(z|x^t)$ and clutter $g^c(z|x^c)$ are given by*

$$g^t(z|x^t) = g_{\tilde{z}}^t(\tilde{z}|\tilde{x}^t) g_a^t(a|\sigma^t) \tag{7}$$

$$g^c(z|x^c) = g_{\tilde{z}}^c(\tilde{z}|\tilde{x}^c) g_a^c(a|\sigma^c) \tag{8}$$

where $g_a^t(a|\sigma^t)$ and $g_a^c(a|\sigma^c)$ are the amplitude likelihood functions for target and clutter, respectively.

***Remark* 1.** *The actual amplitude of the return signal, power and SNR of the receiver input all strongly depend on the distance between sensor and target. However, in the context of radar signal processing, particularly in a radar receiver, there are several gain control techniques [31], for instance sensitivity time control (STC), that would enable reducing the influence of the distance on the returned amplitude. Hence, with the techniques like STC in place, the Assumption (1) is generally valid across many cases.*

Most receivers detect targets by finding the peak of observations that exceed the detection threshold $\tau > 0$. Thus, the amplitude likelihoods for target and clutter after thresholding become

$$g_a^{\tau,t}(a|\sigma^t) = \frac{g_a^t(a|\sigma^t)}{p_D^\tau(\sigma^t)} = \frac{g_a^t(a|\sigma^t)}{\int_\tau^\infty g_a^t(a|\sigma^t)da} \tag{9}$$

$$g_a^{\tau,c}(a|\sigma^c) = \frac{g_a^c(a|\sigma^c)}{p_{FA}^\tau(\sigma^c)} = \frac{g_a^c(a|\sigma^c)}{\int_\tau^\infty g_a^c(a|\sigma^c)da} \tag{10}$$

where $p_D^\tau(\sigma^t)$ and $p_{FA}^\tau(\sigma^c)$ are the probability of detection and probability of false alarm, respectively.

For a given multi-object state $X^t = \left\{x_1^t, \ldots, x_{n_t}^t\right\}$ and clutter state $X^c = \left\{x_1^c, \ldots, x_{n_c}^c\right\}$, the observation set generated from the receiver is of the form

$$Z = \left(\cup_{i=1}^{n_t} \sum(x_i^t)\right) \cup \left(\cup_{i=1}^{n_c} \sum(x_i^c)\right) \tag{11}$$

where $\sum(x_i^t)$ and $\sum(x_i^c)$ are the random finite sets generated by the single target state x_i^t and single clutter state x_i^c, respectively. The generated random finite sets either contain a single observation z_i or are empty.

The multi-object likelihoods for target and clutter, incorporating the AI are then given by [32, 17, 5]

$$\begin{split} f_{k+1}(Z_{k+1}^t | X^t) = \prod_{i=1}^{n_t} (1 - p_D^\tau(\sigma_i^t)) \times \\ \sum_\theta \prod_{i:\theta(i)>0} \frac{p_D^\tau(\sigma_i^t) \cdot g_{\tilde{z}}^t(\tilde{z}_{\theta(i)} | \tilde{x}_i^t) \cdot g_a^{\tau,t}(a_{\theta(i)} | \sigma_i^t)}{1 - p_D^\tau(\sigma_i^t)} \end{split} \tag{12}$$

$$\begin{split} f_{k+1}(Z_{k+1}^c | X^c) = \prod_{i=1}^{n_c} (1 - p_{FA}^\tau(\sigma_i^c)) \times \\ \sum_\phi \prod_{i:\phi(i)>0} \frac{p_{FA}^\tau(\sigma_i^c) \cdot g_{\tilde{z}}^c(\tilde{z}_{\phi(i)} | \tilde{x}_i^c) \cdot g_a^{\tau,c}(a_{\phi(i)} | \sigma_i^c)}{1 - p_{FA}^\tau(\sigma_i^c)} \end{split} \tag{13}$$

where the sums are over all possible associations θ and ϕ between X^t and Z^t and between X^c and Z^c, respectively.

As the whole measurements Z_{k+1} can be expressed as $Z_{k+1} = Z_{k+1}^t \cup Z_{k+1}^c$, the whole multi-object likelihood is given by:

$$f_{k+1}(Z_{k+1} | \ddot{X}) = \sum_{\mathcal{Z} \in \mathcal{F}(Z_{k+1})} f(Z_{k+1} - \mathcal{Z} | X^t) \cdot f(\mathcal{Z} | X^c) \tag{14}$$

where $\ddot{X}$ denotes the joint target/clutter state and the sum is over all the elements of $\mathcal{F}(Z_{k+1})$.

2.3. PHD filter with AI (PHD-AI)

The AI can be incorporated into the standard PHD filter (PHD-AI filter) as outlined in [33]. The PHD-AI filter can then be extended to implement the sequential Monte Carlo (SMC) variant of the PHD filter with the AI as discussed in [34]. In the absence of an *a priori* clutter model, the time-updated PHD of target and clutter states are given by [32, 17, 33]

$$D^t_{k+1|k}(x^t) = b^t_{k+1|k} + \int p^t_S(x') \cdot f^t_{k+1|k}(x^t|x') \cdot D^t_{k|k}(x')dx' \tag{15}$$

$$D^c_{k+1|k}(x^c) = b^c_{k+1|k} + \int p^c_S(x') \cdot f^c_{k+1|k}(x^c|x') \cdot D^c_{k|k}(x')dx' \tag{16}$$

respectively, where $b^t_{k+1|k}$ and $b^c_{k+1|k}$ denote the PHD of new birth target and clutter, respectively. The observation updates for the PHD filter [32, 17, 33] are given by

$$\frac{D^t_{k+1|k+1}(x^t)}{D^t_{k+1|k}(x^t)} = 1 - p^\tau_D(\sigma^t) + \sum_{z\in Z} \frac{p^\tau_D(\sigma^t) g^{\tau,t}_a(a|\sigma^t) g^t_{\tilde{z}}(\tilde{z}|\tilde{x}^t)}{\ddot{\Lambda}_{k+1|k}} \tag{17}$$

$$\frac{D^c_{k+1|k+1}(x^c)}{D^c_{k+1|k}(x^c)} = 1 - p^\tau_{FA}(\sigma^c) + \sum_{z\in Z} \frac{p^\tau_{FA}(\sigma^c) g^{\tau,c}_a(a|\sigma^c) g^c_{\tilde{z}}(\tilde{z}|\tilde{x}^c)}{\ddot{\Lambda}_{k+1|k}} \tag{18}$$

$$\ddot{\Lambda}_{k+1|k} = \left\langle D^t_{k+1|k}, p^\tau_D(\sigma^t) g^{\tau,t}_a(\cdot|\sigma^t) g^t_{\tilde{z}} \right\rangle + \left\langle D^c_{k+1|k}, p^\tau_{FA}(\sigma^c) g^{\tau,c}_a(\cdot|\sigma^c) g^c_{\tilde{z}} \right\rangle \tag{19}$$

where $\langle f, g\rangle$ is the inner product $\int f(x)g(x)dx$.

2.4. CPHD filter with AI (CPHD-AI)

Similar to the PHD-AI extension above, the CPHD filter can also be extended to incorporate the AI [5]. However, when the clutter background is not known, the time-updated joint target/clutter cardinality distribution is given by [32, 17, 5]

$$\ddot{p}_{k+1|k}(\ddot{n}) = \sum_{\ddot{n}\geq 0} \ddot{p}_{k+1|k}(\ddot{n}|\ddot{n}') \cdot \ddot{p}_{k|k}(\ddot{n}') \tag{20}$$

$$\ddot{p}_{k+1|k}(\ddot{n}|\ddot{n}') = \sum_{i=0}^{\ddot{n}} \ddot{p}^{B}_{k+1|k}(\ddot{n}-i) \cdot C_{\ddot{n}',i} \cdot \ddot{\psi}_k^i (1-\ddot{\psi}_k)^{\ddot{n}'-i} \tag{21}$$

$$\ddot{p}^{B}_{k+1|k}(\ddot{n}) = \sum_{n^t+n^c=\ddot{n}} p^{B^t}_{k+1|k}(n^t) \cdot p^{B^c}_{k+1|k}(n^c) \tag{22}$$

$$\ddot{\psi}_k = \frac{\left\langle D^t_{k|k}, p^t_S \right\rangle + \left\langle D^c_{k|k}, p^c_S \right\rangle}{N^t_{k|k} + N^c_{k|k}} \tag{23}$$

where $C_{\ddot{n}',i}$ is the binomial coefficient, $\ddot{p}^{B}_{k+1|k}(\ddot{n})$ is the joint target/clutter birth cardinality distribution, and $N^t_{k|k} = \int D^t_{k|k}(x)dx$ and $N^c_{k|k} = \int D^c_{k|k}(x)dx$. Similar to the PHD filter, the time-updated PHD of target and clutter are given by (15) and (16), respectively.

The observation-updated joint cardinality distribution is given by

$$\frac{\ddot{p}_{k+1|k+1}(\ddot{n})}{\ddot{p}_{k+1|k}(\ddot{n})} = \frac{\ddot{\updownarrow}_{Z_{k+1}}(\ddot{n})}{\sum_{l\geq 0} \ddot{\updownarrow}_{Z_{k+1}}(l) \cdot \ddot{p}_{k+1|k}(l)} \tag{24}$$

$$\ddot{\updownarrow}_{Z_{k+1}}(\ddot{n}) = C_{\ddot{n},m_{k+1}} \cdot \ddot{\phi}_{k+1}^{\ddot{n}-m_{k+1}} \tag{25}$$

$$\ddot{\phi}_{k+1} = \frac{\left\langle D^t_{k|k}, 1-p^\tau_D(\sigma^t) \right\rangle + \left\langle D^c_{k|k}, 1-p^\tau_{FA}(\sigma^c) \right\rangle}{N^t_{k+1|k} + N^c_{k+1|k}} \tag{26}$$

where $N^t_{k+1|k} = \int D^t_{k+1|k}(x)dx$ and $N^c_{k+1|k} = \int D^c_{k+1|k}(x)dx$.

The observation-updated PHD of CPHD filters are then given by

$$\begin{aligned}\frac{D^t_{k+1|k+1}(x^t)}{D^t_{k+1|k}(x^t)} &= \frac{1-p^\tau_D(\sigma^t)}{N^t_{k+1|k} + N^c_{k+1|k}} \cdot \frac{\ddot{G}^{(m_{k+1}+1)}_{k+1|k}(\ddot{\phi}_{k+1})}{\ddot{G}^{(m_{k+1})}_{k+1|k}(\ddot{\phi}_{k+1})} \\ &+ \sum_{z\in Z} \frac{p^\tau_D(\sigma^t) g^{\tau,t}_a(a|\sigma^t) g^t_{\tilde{z}}(\tilde{z}|\tilde{x}^t)}{\ddot{\Lambda}_{k+1|k}}\end{aligned} \tag{27}$$

$$\begin{aligned}\frac{D^c_{k+1|k+1}(x^c)}{D^c_{k+1|k}(x^c)} &= \frac{1-p^\tau_{FA}(\sigma^c)}{N^t_{k+1|k} + N^c_{k+1|k}} \cdot \frac{\ddot{G}^{(m_{k+1}+1)}_{k+1|k}(\ddot{\phi}_{k+1})}{\ddot{G}^{(m_{k+1})}_{k+1|k}(\ddot{\phi}_{k+1})} \\ &+ \sum_{z\in Z} \frac{p^\tau_{FA}(\sigma^c) g^{\tau,c}_a(a|\sigma^c) g^c_{\tilde{z}}(\tilde{z}|\tilde{x}^c)}{\ddot{\Lambda}_{k+1|k}}\end{aligned} \tag{28}$$

$$\ddot{G}^{(l)}_{k+1|k}(\ddot{\phi}_k) = \sum_{\ddot{n}\geq l} \ddot{p}_{k+1|k}(\ddot{n}) \cdot l! \cdot C_{\ddot{n},l} \cdot \ddot{\phi}_k^{\ddot{n}-l} \tag{29}$$

2.5. CBMeMBer filter with AI (CBMeMBer-AI)

The robust CBMeMBer filter proposed in [18] can estimate the unknown clutter intensity and detection profile while filtering. In this paper, we incorporate the AI into the CBMeMBer filter, similar to the approach adopted towards the CPHD-AI filter. For the reasons of brevity, the full details of the CBMeMBer-AI filter is given in Appendix A.

3. Amplitude Information Model

In this section, we consider the specific probability distributions for the target and clutter amplitude observations used in radar signal processing. We first show the amplitude likelihood in a noise-only background and then present the amplitude likelihood in a clutter background.

3.1. Amplitude Likelihood in Noise Background

When processing radar returns, the target power fluctuates for a number of reasons [31], and this is captured by Swerling models with two probability density functions (PDF). These are exponential and fourth-degree Chi-square PDFs. These models can be viewed as special cases of a Chi-square density function with a degree of $2n$, given by

$$p(\sigma|\bar{\sigma}, n) = \frac{n}{\Gamma(n)\bar{\sigma}} \left(\frac{n\sigma}{\bar{\sigma}}\right)^{n-1} \exp\left(\frac{-n\sigma}{\bar{\sigma}}\right), \sigma > 0 \tag{30}$$

where $\bar{\sigma}$ is the mean target power, the exponential corresponds to $n = 1$, while the fourth-degree Chi-square corresponds to $n = 2$.

In the presence of noise, such as thermal noise, the output power of the receiver is a function of the target and the noise returns. Assuming a linear detector, coherent receiver noise has a complex Gaussian amplitude distribution prior to detection, and a Rayleigh distribution after detection. Thus, the probability densities of amplitude a outputted by a linear envelope detector, for noise-only and, target with noise inputs are given by

$$p_n(a) = \frac{2a}{\sigma_n} \exp\left(-\frac{a^2}{\sigma_n}\right) \tag{31}$$

and

$$p_{s+n}(a|a_s) = \frac{2a}{\sigma_n} \exp\left(-\frac{a^2 + a_s^2}{\sigma_n}\right) I_0(2aa_s/\sigma_n) \tag{32}$$

respectively, where $a_s = \sqrt{\sigma}$ is the detected signal voltage, and $I_0(\cdot)$ is the modified Bessel function of the first kind and zero order[1]. The false alarm probability is

$$p_{FA}^{\tau} = \int_{\tau}^{\infty} p_n(a)da = \exp\left(-\frac{\tau^2}{\sigma_n}\right) \tag{33}$$

The amplitude probability density function of the noise-only case after thresholding is

$$p_n^{\tau}(a) = \exp\left(-\frac{a^2 - \tau^2}{\sigma_n}\right) \tag{34}$$

The PDF of amplitude a, which depends on the mean target power, can be derived as

$$p(a|\bar{\sigma}, n) = \int_0^{\infty} p_{s+n}(a|\sqrt{\sigma})p(\sigma|\bar{\sigma}, n)d\sigma \tag{35}$$

[1] Notice that σ_n is the noise power and is not the standard deviation of the noise process defined in signal processing literature

Utilizing characteristic functions and Fourier transform pairs, the PDF for the exponential and fourth-degree Chi-square models can be expressed as

$$p(a|\bar{\sigma}, n=1) = \frac{2a}{\bar{\sigma}+\sigma_n} \exp\left(-\frac{a^2}{\bar{\sigma}+\sigma_n}\right) \tag{36}$$

and

$$\begin{aligned} p(a|\bar{\sigma}, n=2) =& \frac{8a}{(\bar{\sigma}+2\sigma_n)^2} \exp\left(-2\frac{a^2}{\bar{\sigma}+2\sigma_n}\right) \\ & \cdot \left[\sigma_n + \frac{\bar{\sigma}a^2}{\bar{\sigma}+2\sigma_n}\right] \\ \approx & \frac{8a^3}{(\bar{\sigma}+\sigma_n)^2} \exp\left(-2\frac{a^2}{\bar{\sigma}+\sigma_n}\right) \end{aligned} \tag{37}$$

The approximation in (37) is adopted under the large SNR, i.e. $\bar{\sigma} \gg \sigma_n$, that is the power of target signal is significantly larger than the power of the noise of receiver. We define a general Rayleigh probability density function to describe the amplitude in noise background as

$$\mathcal{RL}(a; \sigma, n) = \frac{(2a)^{2n-1}}{(\sigma+\sigma_n)^n} \exp\left(-n\frac{a^2}{\sigma+\sigma_n}\right) \tag{38}$$

And using the approximated expression

$$p_D^{\tau}(\sigma, n) = \exp\left(-n\frac{\tau^2}{\sigma+\sigma_n}\right) \tag{39}$$

the general Rayleigh probability density after thresholding becomes

$$\mathcal{RL}^{\tau}(a; \sigma, n) = \frac{(2a)^{2n-1}}{(\sigma+\sigma_n)^n} \exp\left(-n\frac{a^2-\tau^2}{\sigma+\sigma_n}\right) \tag{40}$$

3.2. Amplitude Likelihood in Clutter Background

Radar clutter returns come from objects that are of no interest to the application in consideration, such as precipitation, vegetation, ground or sea. Clutter statistics can be similar to those of noise, especially when the radar resolution is low. Under this condition, returns from objects of no interest can be viewed as a composition of small, nearly equal-sized scatterers, resulting in Rayleigh distribution. However, as the radar resolution improves and scatterers change, the clutter distributions tend to a have longer tail than the Rayleigh distribution [35]. This can be approximated by the Weibull distribution, which is a commonly used for approximating the natural clutter [36], and given by:

$$p(\sigma|\bar{\sigma}_0, b) = \frac{1}{\bar{\sigma}_0} b\sigma^{b-1} \exp\left(-\frac{\sigma^b}{\bar{\sigma}_0}\right) \tag{41}$$

The exact probability density of the output amplitude of the receiver, when considering returns from target and clutter, can be derived as in (32). It is worth noticing that the clutter power is often significantly larger than that of the noise, and at times larger than that of the returns from targets. In most of the cases, clutter elimination techniques, such as moving target indication (MTI), moving target detection (MTD) or pulse-Doppler processing, may not be as effective as intended to be, and as such, the residual clutter signal will have the same shape as the original distribution [31]. Thus, the probability distribution of the amplitude a outputted by the envelope detector in a clutter background is given by

$$\mathcal{WB}(a; \bar{\sigma}_0, b) = \frac{1}{\bar{\sigma}_0} 2ba^{2b-1} \exp\left(-\frac{a^{2b}}{\bar{\sigma}_0}\right) \tag{42}$$

where $\bar{\sigma}_0$ is the clutter equivalent power of the receiver input. Thus, the false alarm probability in a clutter background is given by

$$p^{\tau}_{FA}(\bar{\sigma}_0, b) = \int_{\tau}^{\infty} p(a|\bar{\sigma}_0, b) da = \exp\left(-\frac{\tau^{2b}}{\bar{\sigma}_0}\right) \tag{43}$$

The corresponding post-threshold probability density of the clutter amplitude is given by

$$\mathcal{WB}^{\tau}(a; \bar{\sigma}_0, b) = \frac{1}{\bar{\sigma}_0} 2ba^{2b-1} \exp\left(-\frac{a^{2b} - \tau^{2b}}{\bar{\sigma}_0}\right) \tag{44}$$

4. The IGGM-RFS-AI Filters

In this section, we first present an inverse Gamma Gaussian (IGG) augmented state model. We then derive the time evolution and observation-updates for the parameters of the IGG model. Finally, we present the IGG mixture implementation of the RFS-AI filters.

4.1. IGG Augmented State Model

In deriving an augmented state model for the IGG, consider the following assumption:

Assumption 2. *The target return power σ_k^t and clutter return power σ_k^c are conditionally independent of the kinematic states $\tilde{x}_k^t$ and $\tilde{x}_k^c$, respectively.*

The augmented target state x_k^t and clutter state x_k^c, conditioned on $Z^k := [\tilde{Z}^k \ a^k]^T$, can be modeled as inverse Gamma Gaussian distributed,

$$\begin{aligned} p(x_k|Z^k) &= p(\sigma_k|a^k) \cdot p(\tilde{x}_k|\tilde{Z}^k) \\ &= \mathcal{IGAM}(\sigma_k; \alpha_{k|k}, \beta_{k|k}) \times \mathcal{N}(\tilde{x}_k; m_{k|k}, P_{k|k}) \\ &= \mathcal{IGG}(x_k; \xi_{k|k}) \end{aligned} \tag{45}$$

where $\mathcal{IGAM}(\sigma_k; \alpha_{k|k}, \beta_{k|k})$ denotes inverse Gamma probability density function defined over $\sigma > 0$ with shape parameter $\alpha > 0$ and scale parameter $\beta > 0$ so that

$$\mathcal{IGAM}(\sigma; \alpha, \beta) = \frac{\beta^\alpha \exp(-\frac{\beta}{\sigma})}{\Gamma(\alpha)\sigma^{\alpha+1}}$$

and $\mathcal{N}(\tilde{x}_k; m_{k|k}, P_{k|k})$ denotes multi-variate Gaussian probability density function defined over the vector $x \in \mathbb{R}^{n_x}$ with mean vector $m \in \mathbb{R}^{n_x}$ and covariance matrix $P \in \mathbb{S}_+^{n_x}$. Therefore,

$$\mathcal{N}(x; m, P) = \frac{\exp\left(-\frac{1}{2}(x-m)^T P^{-1}(x-m)\right)}{\sqrt{(2\pi)^{n_x}|P|}}$$

Furthermore, $\mathbb{S}_{+}^{n_x}$ is the set of symmetric positive semi-definite $n_x \times n_x$ matrices, and $\xi_{k|k} = \{\alpha_{k|k}, \beta_{k|k}, m_{k|k}, P_{k|k}\}$ is the set of prior IGG density parameters.

The IGG augmented state model is used in [8, 9, 10] to estimate the RCS of targets. These approaches incorporate the SNR into the target state and assume amplitude likelihood is Rayleigh. However, the spatial distribution and amplitude likelihood of the clutter process are assumed to be uniform and of the same form as those of the targets. These assumptions are not realistic in practical scenarios. In this paper, we exploit the IGG to model both the target and the clutter states, and consider different likelihood functions for target state filtering and clutter estimation.

4.2. State Transition and Observation Correction

The state transition density that describes the prediction of the target and clutter states between two time steps of t_k and t_{k+1} is $f(x_{k+1}|x_k)$. This time evolution involves solving the following Chapman-Kolmogorov equation:

$$
\begin{aligned}
p(x_{k+1}|Z^k) &= \int f(x_{k+1}|x_k) p(x_k|Z^k) dx \\
&= \int f_\sigma(\sigma_{k+1}|\sigma_k) \mathcal{IGAM}(\sigma_k; \alpha_{k|k}, \beta_{k|k}) d\sigma \\
&\times \int f_{\tilde{x}}(\tilde{x}_{k+1}|\tilde{x}_k) \mathcal{N}(\tilde{x}_k; m_{k|k}, P_{k|k}) d\tilde{x}_k
\end{aligned}
\tag{46}
$$

Assumption 3. *Kinematic states of targets and clutters follow a linear Gaussian dynamical model given by*

$$\tilde{x}_{k+1} = F_{k+1}\tilde{x}_k + w_{k+1} \tag{47}$$

where w_{k+1} is the zero mean Gaussian process noise with the covariance of Q_{k+1}, and F_{k+1} is the state transition matrix. Thus, the corresponding state transition density is given by

$$f_{\tilde{x}}(\tilde{x}_{k+1}|\tilde{x}_k) = \mathcal{N}(\tilde{x}_{k+1}; F_{k+1}\tilde{x}_k, Q_{k+1}) \tag{48}$$

With this, the prediction for the kinematic state becomes

$$\begin{aligned}&\int \mathcal{N}(\tilde{x}_{k+1}; F_{k+1}\tilde{x}_k, Q_{k+1})\mathcal{N}(\tilde{x}_k; m_{k|k}, P_{k|k})d\tilde{x}_k \\ &= \mathcal{N}(\tilde{x}_{k+1}; m_{k+1|k}, P_{k+1|k})\end{aligned} \tag{49}$$

where $m_{k+1|k} = F_{k+1}m_{k|k}$ and $P_{k+1|k} = F_{k+1}P_{k|k}F_{k+1}^T + Q_{k+1}$

The integral corresponding to the return power is non-trivial to solve. To address this, an exponential forgetting method [37] can be adopted with a forgetting factor of $\upsilon_{k|k}$. With this, the return power prediction becomes

$$\beta_{k+1|k} = \frac{\beta_{k|k}}{\upsilon_{k|k}}, \alpha_{k+1|k} = \frac{\alpha_{k|k} + \upsilon_{k|k} - 1}{\upsilon_{k|k}} \tag{50}$$

This prediction has an effective window of length w_e, given by

$$w_e = \frac{1}{1 - 1/\upsilon_{k|k}} = \frac{\upsilon_{k|k}}{\upsilon_{k|k} - 1}$$

The statistics of σ are

$$E[\sigma_{k+1}] = \frac{\beta_{k+1|k}}{\alpha_{k+1|k} - 1} = \frac{\beta_{k|k}}{\alpha_{k|k} - 1} = E[\sigma_k] \tag{51}$$

and

$$\begin{aligned} Var[\sigma_{k+1}] &= \frac{\beta_{k+1|k}}{(\alpha_{k+1|k} - 1)^2(\alpha_{k+1|k} - 1)} \\ &= \frac{\upsilon\beta_{k|k}^2}{(\alpha_{k|k} - 1)^2(\alpha_{k|k} - 2 + 1 - \upsilon)} \\ &> \frac{\upsilon\beta_{k|k}^2}{(\alpha_{k|k} - 1)^2(\alpha_{k|k} - 2)} \\ &= \upsilon \cdot Var[\sigma_k] \end{aligned} \tag{52}$$

Equations (51) and (52) imply that the prediction corresponds to keeping the mean value constant while increasing the variance. Furthermore, we set $\xi_{k+1|k}$, set of time-updated IGG density parameters, as

$$\xi_{k+1|k} = \left\{\alpha_{k+1|k}, \beta_{k+1|k}, m_{k+1|k}, P_{k+1|k}\right\}$$

In the following, we derive the observation corrections of the IGG density parameters with Gaussian kinematic likelihood, Rayleigh target amplitude likelihood, and Weibull clutter amplitude likelihood. These updates can be induced into the PHD filter, the CPHD filter, and the CBMeMBer filter to form closed recursions in Section 4.3, 4.4, and 4.5, respectively.

The posterior state density $p(x_{k+1}|z_{k+1})$ is given by

$$\begin{aligned} p(x_{k+1}|z_{k+1}) &= \frac{1}{K} \times g(z_{k+1}|x_{k+1})p(x_{k+1}|z_k) \\ &\propto g_a(a_{k+1}|\sigma_{k+1})\mathcal{IGAM}(\sigma_{k+1}; \alpha_{k+1|k}, \beta_{k+1|k}) \\ &\times g_{\tilde{z}}(\tilde{z}_{k+1}|\tilde{x}_{k+1})\mathcal{N}(\tilde{x}_{k+1}; m_{k+1|k}, P_{k+1|k}) \end{aligned} \tag{53}$$

where the individual measurement likelihood $g_z(z_{k+1}|x_{k+1})$ in (53) describes the relation between the measurements $z_{k+1} \in Z_{k+1}$ generated by a target or a clutter and the corresponding state x_{k+1}, and K is the normalizing factor given by

$$K = \int g(z_{k+1}|x)p(x|z_k)dx$$

Assumption 4. *The sensor has a linear Gaussian measurement model for kinematic state. That is,*

$$\tilde{z}_{k+1} = H_{k+1}\tilde{x}_{k+1} + e_{k+1} \tag{54}$$

where e_{k+1} is a white Gaussian noise with covariance R_{k+1}, and H_{k+1} is the measurement matrix. The likelihood function for the kinematic state is given by

$$g_{\tilde{z}}(\tilde{z}_{k+1}|\tilde{x}_{k+1}) = \mathcal{N}(\tilde{z}_{k+1}; H_{k+1}\tilde{x}_{k+1}, R_{k+1}) \tag{55}$$

Using the Gaussian identity, the correction for the kinematic state becomes

$$\begin{aligned}&\mathcal{N}(\tilde{z}_{k+1}; H_{k+1}\tilde{x}_{k+1}, R_{k+1})\mathcal{N}(\tilde{x}_{k+1}; m_{k+1|k}, P_{k+1|k})\\&= \mathcal{N}(\tilde{x}_{k+1}; m_{k+1|k+1}, P_{k+1|k+1})\mathcal{N}(\tilde{z}_{k+1}; z_{k+1|k}, S_{k+1|k})\end{aligned} \tag{56}$$

where $z_{k+1|k} = H_{k+1}m_{k+1|k}$ and $S_{k+1|k} = H_{k+1}P_{k+1|k}H_{k+1}^T + R_{k+1}$.

The corresponding Kalman gain, Kalman mean and Kalman variance updates are

$$K_{k+1|k} = P_{k+1|k}H_{k+1}^T \left(S_{k+1|k}\right)^{-1} \tag{57}$$

$$m_{k+1|k+1} = m_{k+1|k} + K_{k+1|k}z_{k+1|k} \tag{58}$$

$$P_{k+1|k+1} = \left(I_{n_x \times n_x} - K_{k+1|k}H_{k+1}\right) P_{k+1|k} \tag{59}$$

For a large target return power, the amplitude likelihood after thresholding $g_a^\tau(a_{k+1}|\sigma_{k+1}) = \mathcal{RL}^\tau(a_{k+1}; \sigma_{k+1}, n)$. Then, the posterior density is derived as

$$\begin{aligned}&\mathcal{RL}^\tau(a_{k+1}; \sigma_{k+1}, n)\mathcal{IGAM}(\sigma_{k+1}; \alpha_{k+1|k}, \beta_{k+1|k})\\&= K_{\mathcal{RL}^\tau}(a_{k+1}; \alpha_{k+1|k}, \beta_{k+1|k}, n)\mathcal{IGAM}(\sigma_{k+1}; \alpha_{k+1|k+1}, \beta_{k+1|k+1})\end{aligned} \tag{60}$$

The posterior inverse Gamma parameters are given by

$$\beta_{k+1|k+1} = \beta_{k+1|k} + na^2 - n\tau^2,\ \alpha_{k+1|k+1} = \alpha_{k+1|k} + n$$

And the innovation factor of the target amplitude measurement is

$$K_{\mathcal{RL}^\tau}(a_{k+1}; \alpha_{k+1|k}, \beta_{k+1|k}, n) = \frac{(2a_{k+1})^{2n-1}\left[(n-1)\alpha_{k+1|k}^2 + \alpha_{k+1|k}\right]\beta_{k+1|k}^{\alpha_{k+1|k}}}{(\beta_{k+1|k} + na_{k+1}^2 - n\tau^2)^{\alpha_{k+1|k}+n}} \tag{61}$$

For clutter return power, the amplitude likelihood after thresholding $g_a^\tau(a_{k+1}|\sigma_{k+1}) = \mathcal{WB}^\tau(a_{k+1};\sigma_{k+1},b)$. the posterior density is derived by

$$
\begin{aligned}
&\mathcal{WB}^\tau(a_{k+1};\sigma_{k+1},b)\mathcal{IGAM}(\sigma_{k+1|k};\alpha_{k+1|k},\beta_{k+1|k})\\
&= K_{\mathcal{WB}^\tau}(a_{k+1};\alpha_{k+1|k},\beta_{k+1|k},b)\mathcal{IGAM}(\sigma_{k+1};\alpha_{k+1|k+1},\beta_{k+1|k+1})
\end{aligned} \tag{62}
$$

The posterior inverse Gamma parameters are given by

$$
\beta_{k+1|k+1} = \beta_{k+1|k} + a^{2b} - \tau^{2b},\ \ \alpha_{k+1|k+1} = \alpha_{k+1|k} + 1
$$

And the innovation factor of the clutter amplitude measurement is

$$
K_{\mathcal{WB}^\tau}(a_{k+1};\alpha_{k+1|k},\beta_{k+1|k},b) = \frac{2ba_{k+1}^{2b-1}\alpha_{k+1|k}\beta_{k+1|k}^{\alpha_{k+1|k}}}{(\beta_{k+1|k} + a_{k+1}^{2b} - \tau^{2b})^{\alpha_{k+1|k}+1}} \tag{63}
$$

Let

$$
\begin{aligned}
&\mathcal{L}^t(z_{k+1};\xi_{k+1|k},n) =\\
&\qquad \mathcal{N}(\tilde{z}_{k+1};z_{k+1|k},S_{k+1|k})K_{\mathcal{RL}^\tau}(a_{k+1};\alpha_{k+1|k},\beta_{k+1|k},n)
\end{aligned} \tag{64}
$$

$$
\begin{aligned}
&\mathcal{L}^c(z_{k+1};\xi_{k+1|k},b) =\\
&\qquad \mathcal{N}(\tilde{z}_{k+1};z_{k+1|k},S_{k+1|k})K_{\mathcal{WB}^\tau}(a_{k+1};\alpha_{k+1|k},\beta_{k+1|k},b)
\end{aligned} \tag{65}
$$

Furthermore, $\xi_{k+1|k+1}$, the set of observation-updated IGG density parameters, is set to

$$
\xi_{k+1|k+1} = \left\{\alpha_{k+1|k+1},\beta_{k+1|k+1},m_{k+1|k+1},P_{k+1|k+1}\right\}
$$

4.3. The IGGM-PHD-AI Filter

In order to derive prediction and correction equations for the IGGM-PHD-AI filter, a number of assumptions are made here in addition to the assumptions already described.

Assumption 5. *The current estimated PHD $D_{k|k}$ is an unnormalized mixture of IGG distributions. That is,*

$$
D_{k|k}^t(x_k^t) \approx \sum_{j=1}^{J_{k|k}^t} \omega_{k|k}^{t,(j)}\mathcal{IGG}(x_k^t;\xi_{k|k}^{t,(j)}) \tag{66}
$$

$$D^c_{k|k}(x^c_k) \approx \sum_{j=1}^{J^c_{k|k}} \omega^{c,(j)}_{k|k} \mathcal{IGG}(x^c_k; \xi^{c,(j)}_{k|k}) \tag{67}$$

where $J^*_{k|k}$ is the number of components, $\omega^{*,(j)}_{k|k}$ is the weight of the j-th component, and $\xi^{*,(j)}_{k|k}$ is the density parameter of the j-th component.

Assumption 6. *The intensity of the birth target and birth clutter are also an unnormalized mixture of IGG distributions with parameter $\left\{\omega^{t,(i)}_B, \xi^{t,(j)}_B\right\}_{i=1}^{b^t_{k+1}}$ and $\left\{\omega^{c,(i)}_B, \xi^{c,(j)}_B\right\}_{i=1}^{b^c_{k+1}}$, respectively.*

Assumption 7. *The survival probability is state independent, i.e., $p^t_S(x^t) = p^t_S, p^c_S(x^c) = p^c_S$.*

Utilizing (15), (16), (46) and Assumption 3, the time-updated PHD parameters are given by

$$D^t_{k+1|k}(x^t_{k+1}) = \sum_{j=1}^{J^t_{k|k}} \omega^{t,(j)}_{k+1|k} \mathcal{IGG}(x^t_{k+1}; \xi^{t,(j)}_{k+1|k}) + \sum_{i=1}^{b^t_{k+1}} \omega^{t,(i)}_B \mathcal{IGG}(x^t_B; \xi^{t,(j)}_B) \tag{68}$$

$$D^c_{k+1|k}(x^c_{k+1}) = \sum_{j=1}^{J^c_{k|k}} \omega^{c,(j)}_{k+1|k} \mathcal{IGG}(x^c_{k+1}; \xi^{c,(j)}_{k+1|k}) + \sum_{i=1}^{b^c_{k+1}} \omega^{c,(i)}_B \mathcal{IGG}(x^c_B; \xi^{c,(j)}_B) \tag{69}$$

where $\omega^{t,(j)}_{k+1|k} = p^t_S \omega^{t,(j)}_{k|k}, \omega^{c,(j)}_{k+1|k} = p^c_S \omega^{c,(j)}_{k|k}$. $\xi^{t,(j)}_{k+1|k}$ and $\xi^{c,(j)}_{k+1|k}$ are derived as in (49)–(52).

Utilizing (17), (18), (53) and Assumption 4, the observation-updated PHD are given by

$$\begin{aligned} D^t_{k+1|k+1}(x^t_{k+1}) = &\sum_{j=1}^{J^t_{k+1|k}} \omega^{t,(j)}_{k+1|k+1} \mathcal{IGG}(x^t_{k+1}; \xi^{t,(j)}_{k+1|k+1}) \\ &+ \sum_{m=1}^{M_{k+1}} \sum_{j=1}^{J^t_{k+1|k}} \omega^{t,(m,j)}_{k+1|k+1} \mathcal{IGG}(x^t_{k+1}; \xi^{t,(m,j)}_{k+1|k+1}) \end{aligned} \tag{70}$$

$$\begin{aligned} D^c_{k+1|k+1}(x^c_{k+1}) = & \sum_{j=1}^{J^c_{k+1|k}} \omega^{c,(j)}_{k+1|k+1} \mathcal{IGG}(x^c_{k+1}; \xi^{c,(j)}_{k+1|k+1}) \\ & + \sum_{m=1}^{M_{k+1}} \sum_{j=1}^{J^c_{k+1|k}} \omega^{c,(m,j)}_{k+1|k+1} \mathcal{IGG}(x^c_{k+1}; \xi^{c,(m,j)}_{k+1|k+1}) \end{aligned} \tag{71}$$

where

$$\omega^{t,(j)}_{k+1|k+1} = \left(1 - p^{\tau}_D(\hat{\sigma}^t)\right) \omega^{t,(j)}_{k+1|k}$$

$$\begin{aligned} \ddot{\Lambda}^{(m)}_{k+1|k} = & \sum_{j=1}^{J^t_{k+1|k}} p^{\tau}_D(\hat{\sigma}^t) \mathcal{L}^t(z^{(m)}_{k+1}; \xi^{t,(j)}_{k+1|k}, n) \omega^{t,(j)}_{k+1|k} \\ & + \sum_{j=1}^{J^c_{k+1|k}} p^{\tau}_{FA}(\hat{\sigma}^c) \mathcal{L}^t(z^{(m)}_{k+1}; \xi^{c,(j)}_{k+1|k}, n) \omega^{c,(j)}_{k+1|k} \end{aligned} \tag{72}$$

$$\omega^{c,(j)}_{k+1|k+1} = \left(1 - p^{\tau}_D(\hat{\sigma}^c)\right) \omega^{c,(j)}_{k+1|k}$$

$$\omega^{t,(m,j)}_{k+1|k+1} = \frac{\mathcal{L}^t(z^{(m)}_{k+1}; \xi^{t,(j)}_{k+1|k}, n)}{\ddot{\Lambda}^{(m)}_{k+1|k}} p^{\tau}_D(\hat{\sigma}^t) \omega^{t,(j)}_{k+1|k}$$

$$\omega^{c,(m,j)}_{k+1|k+1} = \frac{\mathcal{L}^c(z^{(m)}_{k+1}; \xi^{c,(j)}_{k+1|k}, b)}{\ddot{\Lambda}^{(m)}_{k+1|k}} p^{\tau}_{FA}(\hat{\sigma}^c) \omega^{c,(j)}_{k+1|k}$$

$\xi^{t,(j)}_{k+1|k+1} = \xi^{t,(j)}_{k+1|k}$ and $\xi^{c,(j)}_{k+1|k+1} = \xi^{c,(j)}_{k+1|k}$. $\xi^{t,(m,j)}_{k+1|k+1}$ and $\xi^{c,(m,j)}_{k+1|k+1}$ are derived as in Equations (56)–(62).

4.4. The IGGM-CPHD-AI Filter

The IGGM-CPHD-AI filter also follows Assumptions 2–7. The time-updated parameters

$$\left\{\omega^{t,(j)}_{k+1|k}, \xi^{t,(j)}_{k+1|k}, \omega^{t,(j)}_{k+1|k}, \xi^{c,(j)}_{k+1|k}\right\}$$

are same as the parameters of the IGGM-PHD-AI filter and the factor for the time-updated joint target/clutter cardinality distribution is given by

$$\ddot{\psi}_k = \frac{p_S^t \sum_{j=1}^{J_{k|k}^t} \omega_{k|k}^{t,(j)} + p_S^c \sum_{j=1}^{J_{k|k}^c} \omega_{k|k}^{c,(j)}}{\sum_{j=1}^{J_{k|k}^t} \omega_{k|k}^{t,(j)} + \sum_{j=1}^{J_{k|k}^c} \omega_{k|k}^{c,(j)}} \tag{73}$$

The factor for the observation-updated joint target/clutter cardinality distribution is given by

$$\ddot{\phi}_{k+1} = 1 - \frac{p_D^\tau(\hat{\sigma}^t) \sum_{j=1}^{J_{k+1|k}^t} \omega_{k+1|k}^{t,(j)} + p_{FA}^\tau(\hat{\sigma}^c) \sum_{j=1}^{J_{k+1|k}^c} \omega_{k+1|k}^{c,(j)}}{\sum_{j=1}^{J_{k+1|k}^t} \omega_{k+1|k}^{t,(j)} + \sum_{j=1}^{J_{k+1|k}^c} \omega_{k+1|k}^{c,(j)}} \tag{74}$$

The observation-undetected parameters of the CPHD filter are given by

$$\begin{aligned} \omega_{k+1|k+1}^{t,(j)} =& \frac{(1 - p_D^\tau(\hat{\sigma}^t))\, \omega_{k+1|k}^{t,(j)}}{\sum_{j=1}^{J_{k+1|k}^t} \omega_{k+1|k}^{t,(j)} + \sum_{j=1}^{J_{k+1|k}^c} \omega_{k+1|k}^{c,(j)}} \\ & \times \frac{\ddot{G}_{k+1|k}^{(m_{k+1}+1)}(\ddot{\phi}_{k+1})}{\ddot{G}_{k+1|k}^{(m_{k+1})}(\ddot{\phi}_{k+1})} \end{aligned} \tag{75}$$

$$\begin{aligned} \omega_{k+1|k+1}^{c,(j)} =& \frac{(1 - p_{FA}^\tau(\hat{\sigma}^c))\, \omega_{k+1|k}^{c,(j)}}{\sum_{j=1}^{J_{k+1|k}^t} \omega_{k+1|k}^{t,(j)} + \sum_{j=1}^{J_{k+1|k}^c} \omega_{k+1|k}^{c,(j)}} \\ & \times \frac{\ddot{G}_{k+1|k}^{(m_{k+1}+1)}(\ddot{\phi}_{k+1})}{\ddot{G}_{k+1|k}^{(m_{k+1})}(\ddot{\phi}_{k+1})} \end{aligned} \tag{76}$$

Furthermore,

$$\xi_{k+1|k+1}^{t,(j)} = \xi_{k+1|k}^{t,(j)}$$

and

$$\xi_{k+1|k+1}^{c,(j)} = \xi_{k+1|k}^{c,(j)}$$

Observation-detected parameters

$$\left\{\omega_{k+1|k+1}^{t,(m,j)}, \xi_{k+1|k+1}^{t,(m,j)}, \omega_{k+1|k+1}^{c,(m,j)}, \xi_{k+1|k+1}^{c,(m,j)}\right\}$$

also are as same as the parameters of IGGM-PHD-AI filter.

4.5. The IGGM-CBMeMBer-AI Filter

We also provide the full details of the IGGM-CBMeMBer-AI filter in Appendix B.

4.6. Pruning and Merging

The IGGM implementation of RFS-AI filters needs pruning and merging to reduce the exponential growth of the number of IGG components. The pruning procedure is similar to that of the standard GM implementation, where the relative weights of the IGGM components are considered, and components with negligible weight will be discarded [38].

A method for merging the mixtures of exponential family distributions is described in [37] and [39]. We briefly review this method prior to applying it to IGGM. When merging multiple Gaussian mixtures, the primary task is to determine the merging criterion, which is usually found by calculating the distance between two distributions and comparing it to the merging threshold. An effective distance measure is the symmetrized Kullback-Leibler divergence (SKLD) defined by

$$\begin{aligned}\mathcal{D}_{SKL}(p(x), q(x) &= \mathcal{D}_{KL}(p||q) + \mathcal{D}_{KL}(q||p) \\ &= \int p(x) \log \frac{p(x)}{q(x)} dx + \int q(x) \log \frac{q(x)}{p(x)} dx\end{aligned} \tag{77}$$

Let $p(\sigma)$ and $q(\sigma)$ be defined as

$$p(\sigma) = \mathcal{IGAM}(\sigma; \alpha_1, \beta_1) \tag{78}$$

$$q(\sigma) = \mathcal{IGAM}(\sigma; \alpha_2, \beta_2) \tag{79}$$

Similar to the derivation of the SKLD of Gamma distributions described in [39], the SKLD between $p(\cdot)$ and $q(\cdot)$ is

$$\mathcal{D}_{SKL}(p(\sigma), q(\sigma)) = (\alpha_1 - \alpha_2)(\psi_0(\alpha_1) - \psi_0(\alpha_2) + \log\frac{\beta_2}{\beta_1}) + (\beta_1 - \beta_2)(\frac{\alpha_2}{\beta_2} - \frac{\alpha_1}{\beta_1}) \tag{80}$$

The merging criterion of IGGM should be defined over both σ and $\tilde{x}$, and the following bi-threshold criterion could be used

$$(\mathcal{D}^{\sigma}_{SKL}(p(\sigma), q(\sigma)) < U_{\sigma})\,\&\,\left(\mathcal{D}^{\tilde{x}}_{SKL}(p(\tilde{x}), q(\tilde{x})) < U_{\tilde{x}}\right) \tag{81}$$

The merging criteria $\mathcal{D}^{\tilde{x}}_{SKL}(p(\tilde{x}), q(\tilde{x}))$ of kinematic state $\tilde{x}$, which is Gaussian distributed, is given in [38].

The merging is performed by minimizing the Kullback-Leibler divergence between the mixture of distributions p^{Σ} and the merged distribution $\bar{p}$, which is given by

$$\bar{p}(x) = \arg\min_{\bar{p}} \mathcal{D}_{KL}(p^{\Sigma}||\bar{p}) = \arg\max_{\bar{p}} \int p^{\Sigma}(x)\log(\bar{p}(x))dx \tag{82}$$

Let $p^{\Sigma}(\sigma)$ and $\bar{p}(\sigma)$ be defined as

$$p^{\Sigma}(\sigma) = \sum_{i=1}^{N} \omega_i \mathcal{IGAM}(\sigma; \alpha_i, \beta_i) \tag{83}$$

$$\bar{p}(\sigma) = \bar{\omega}\mathcal{IGAM}(\sigma; \alpha, \beta) \tag{84}$$

where $\bar{\omega} = \sum_{i=1}^{N} \omega_i$, $\beta = \frac{\bar{\omega}\alpha}{\sum_{i=1}^{N} \omega \frac{\alpha_i}{\beta_i}}$ and α is the solution to

$$\log\alpha - \psi_0(\alpha) + \frac{1}{\bar{\omega}}\sum_{i=1}^{N}\omega_i(\psi_0(\alpha_i) - \log\beta_i) - \log\left(\frac{1}{\bar{\omega}}\sum_{i=1}^{N}\omega_i\frac{\alpha_i}{\beta_i}\right) = 0 \tag{85}$$

Table 1: Simulation Scenarios Covered by the Evaluation.

Scenario	**Spatial Distribution**	**Amplitude Distribution**	**Clutter Rate**
S_1	Uniform	Rayleigh	40
S_2	Non-Uniform	Rayleigh	40
S_3	Uniform	Weibull	40
S_4	Non-Uniform	Weibull	40
S_5	Uniform	Weibull	160

5. Simulation Results

We consider a number of realistic scenarios to demonstrate the performance of the IGGM multi-object filters with amplitude information. We outline these scenarios in Table 1. In all scenarios, we consider the case of linear multi-object tracking with 12 targets within the region of surveillance defined by $[-1000\text{m}, +1000\text{m}] \times [-1000\text{m}, +1000\text{m}]$. All targets follow the linear Gaussian and constant velocity motion model given by the following state transition:

$$x_k = \begin{bmatrix} 1 & T & 0 & 0 \\ 0 & 1 & 0 & 0 \\ 0 & 0 & 1 & T \\ 0 & 0 & 0 & 1 \end{bmatrix} x_{k-1} + \begin{bmatrix} T^2/2 & 0 \\ T & 0 \\ 0 & T^2/2 \\ 0 & T \end{bmatrix} \nu_k \tag{86}$$

where x_k represents the target state vector at time k and $T = 1\text{s}$ is the sampling period. The process noise ν_k is a zero mean white Gaussian noise with standard deviation of 5m/s^2. The linear observation model of the kinematic state is given by

$$z_k = \begin{bmatrix} 1 & 0 & 0 & 0 \\ 0 & 0 & 1 & 0 \end{bmatrix} x_k + \begin{bmatrix} 1 & 0 \\ 0 & 1 \end{bmatrix} w_k \tag{87}$$

where the measurement noise w_k is an independent zero mean white Gaussian noise with standard deviations 10m. In addition, the measurement noise is also independent of the process noise.

The length of the simulation is 50 seconds. The targets appear at time 1s, 10s, 20s, and 30s with two targets disappearing simultaneously at time 40s. We show the trajectories of these targets in Fig. 1.

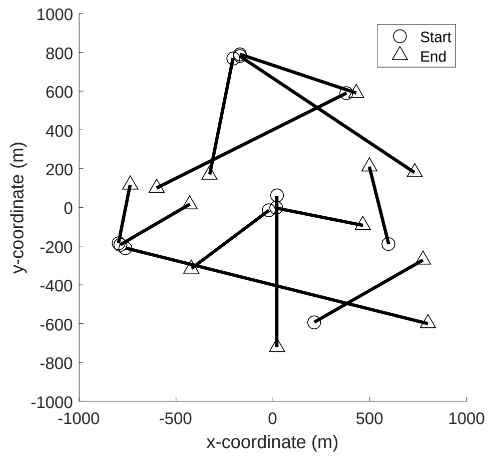

Figure 1: Target Trajectories in the xy Plane.

In the following sub-sections, we discuss the results of our evaluation for each scenario. We compare the IGGM-CPHD-AI filter against the standard GM-CPHD [23], GM-CPHD with the amplitude information (GM-CPHD-AI) [5], and the BGM-CPHD filters for unknown background [40], across all scenarios. In addition to this, we also evaluate the performance of the IGGM-CBMeMBer-AI filter against GM-CBMeMBer, GM-CBMeMBer-AI and BGM-CBMeMBer filters, for Scenarios S_3-S_5.

The parameters used to configure the filters are given in Table 2. The prior clutter rates in the GM-CPHD filter and the GM-CPHD-AI filter are set to 40. The target equivalent return power is 20dB, which yields the detection probability is $p_D = 0.9775$. The pruning and merging procedure are performed using the thresholds stated in Table 2.

Table 2: Parameter Values Used in Filtering.

Parameter	**Value**
The survival probability p_S of actual targets	0.99
The false alarm probability p_{FA}	0.10
Detection threshold τ	2.146
Maximum Gaussian components J_{max}	500
Pruning Threshold T	10^{-5}
Merging Threshold U	4
Birth target process	Poisson RFS
Birth target process intensity $\omega_B^{(i)}$	0.03
Birth target process kinematic state density $p_B^{(i)}(x)$	$\mathcal{N}(x; m_B^{(i)}, P_B)$ $m_B^{(1)} = [0; 0; 0; 0]^T$ $m_B^{(2)} = [200; 0; -600; 0]^T$ $m_B^{(3)} = [-800; 0; -200; 0]^T$ $m_B^{(4)} = [-200; 0; 800; 0]^T$ $m_B^{(5)} = [400; 0; 600; 0]^T$ $m_B^{(6)} = [600; 0; -200; 0]^T$ $P_B = \mathrm{diag}([10; 10; 10; 10]^T)^2$

5.1. Scenario S_1

In this scenario, we use 400 Rayleigh clutter generators with uniform spatial distribution to generate observations of clutter. With 0.1 false alarm probability, the mean clutter rate after detection is 40. Thus, the GM-CPHD filter and the GM-CPHD-AI filter match the clutter rate. The output of the IGGM-CPHD-AI filter in a noisy background is shown in Fig. 2, giving the x and y coordinates of the true and estimated positions against time. As can be observed, the IGGM-CPHD-AI filter produces accurate estimates of the target positions. Fig. 3 shows the average optimal subpattern assignment (OSPA) miss distance [41] with parameters $p = 1$ and $c = 300$m for various filters across 100 Monte Carlo runs. It can be noticed that the GM-CPHD-AI filter delivers the best OSPA miss distance, followed by the GM-CPHD, BGM-CPHD and the IGGM-CPHD-AI filters. Clearly, incorporating the AI as part of the GM-CPHD has improved the performance of GM-CPHD. Although the performance of the IGGM-CPHD-AI is inferior to GM-CPHD-AI and GM-CPHD filters, it still outperforms the BGM-CPHD filter.

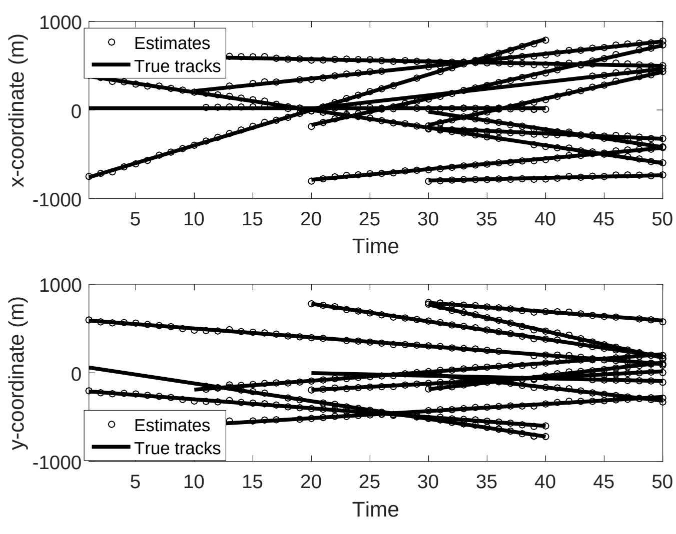

Figure 2: IGGM-CPHD-AI filter: Variation of true tracks and their estimates against time in the x and y coordinate space (for S_1).

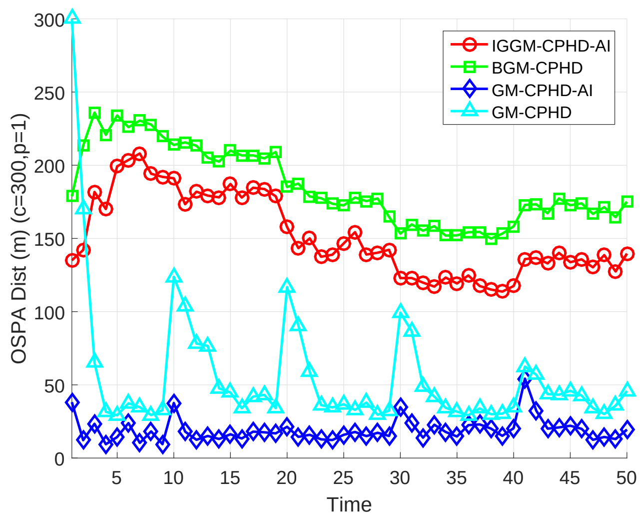

Figure 3: Variation of OSPA miss distance against time for GM-CPHD, GM-CPHD-AI, BGM-CPHD, and IGGM-CPHD-AI filters in uniform Rayleigh background (S_1).

5.2. Scenario S_2

In this scenario, the actual clutter rate is still 40. The spatial distribution under this scenario is the sum of four Gaussian spatial distributions with the center positions of [0m, 0m], [-500m, -500m], [500m, -500m], and [0m, 500m], and with the variance of [100m^2, 100m^2]. We show the resulting performance in Fig. 4. From the results, it is apparent that the IGGM-CPHD-AI filter delivers the best performance, followed by the GM-CPHD-AI and other filters. The performance of the GM-CPHD and GM-CPHD-AI are sub-optimal to that of the IGGM-CPHD-AI, primarily due to the use of an incorrect model for the spatial distribution of the clutter. However, GM-CPHD-AI performs better than the GM-CPHD with the AI incorporated.

5.3. Scenario S_3

In this scenario, the amplitude of clutter comes from Weibull generators with the parameter $b = 0.8$. The clutter power and detection threshold are the

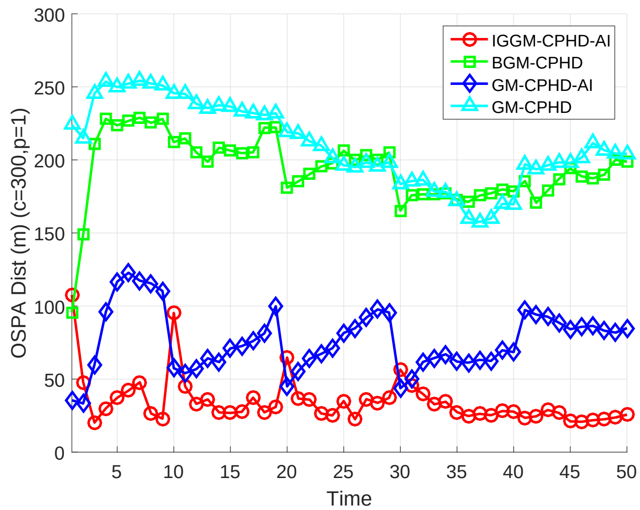

Figure 4: Variation of OSPA miss distance against time for GM-CPHD, GM-CPHD-AI, BGM-CPHD, and IGGM-CPHD-AI filters in non-uniform Rayleigh background (S_2).

same as in Scenario S_1, but with the actual value for the false alarm probability increased to $p_{FA} = 0.39$. To render a fair comparison and to fit the a priori clutter model with 40 clutter rate, the number of clutter generators is decreased from 400 to 100. The resulting performance of various filters, in terms of OSPA miss distance, is shown in Fig. 5. In 5(a), we show the performance of various CPHD filters while we show the performance of various CBMeMBer filters in Fig. 5(b). It is obvious that the GM-CPHD filter and the GM-CBMeMBer filter outperform the methods, which have the clutter estimation, since the prior spatial distribution of clutter in these two filter matches the scenario configuration. Comparing Fig. 3 and 5(a), reveals that an incorrect amplitude model, despite having same spatial distributions, is likely to lead to loss of performance.

5.4. Scenario S_4

We exploit the Weibull clutter generator with non-uniform spatial distribution in this scenario. The performance results for various CPHD and CBMeMBer filters are presented in Figures 6(a) and 6(b), respectively. In both cases,

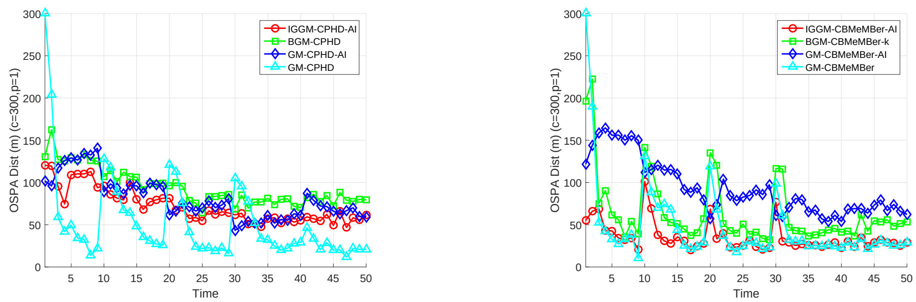

(a) Variations of OSPA miss distance for the GM-CPHD, GM-CPHD-AI, BGM-CPHD, and IGGM-CPHD-AI filters

(b) Variations of OSPA miss distance for the GM-CBMeMBer, GM-CBMeMBer-AI, BGM-CBMeMBer, and IGGM-CBMeMBer-AI filters

Figure 5: Variation of OSPA miss distance with time for various filters in uniform Weibull background (S_3).

it can be observed that IGGM-CPHD-AI and the IGGM-CBMeMBer-AI filters can handle the non-uniform spatial distribution of the clutter much better than other filters.

5.5. Scenario S_5

For this scenario, we maintain 400 Weibull clutter generators to form a high clutter level. The resulting performance is shown in Fig. 7. It can be noticed that almost all but the IGGM-CPHD-AI filter suffer a large loss of performance, with their performance not improving with time at all. From the results, it is also evident that the proposed filter is more robust in cases where clutter background is strong and AI from target and clutter are non-distinguishable.

6. Conclusions

In this paper, we have demonstrated how the AI can be incorporated into the multi-object Bayesian filter. In particular, we have used the inverse Gamma Gaussian model to capture the return powers of the target and clutter. By developing a suite of computationally tractable approximations of these filters

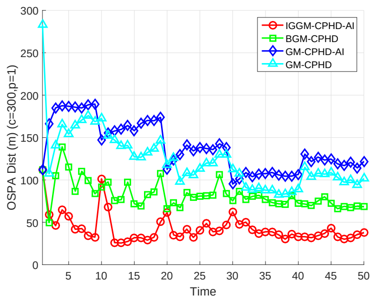

(a) Variations of OSPA miss distance for the GM-CPHD, GM-CPHD-AI, BGM-CPHD, and IGGM-CPHD-AI filters

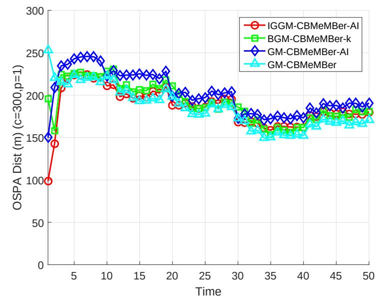

(b) Variations of OSPA miss distance for the GM-CBMeMBer, GM-CBMeMBer-AI, BGM-CBMeMBer, and IGGM-CBMeMBer-AI filters

Figure 6: Variation of OSPA miss distance with time for various filters in nonuniform Weibull background (S_4).

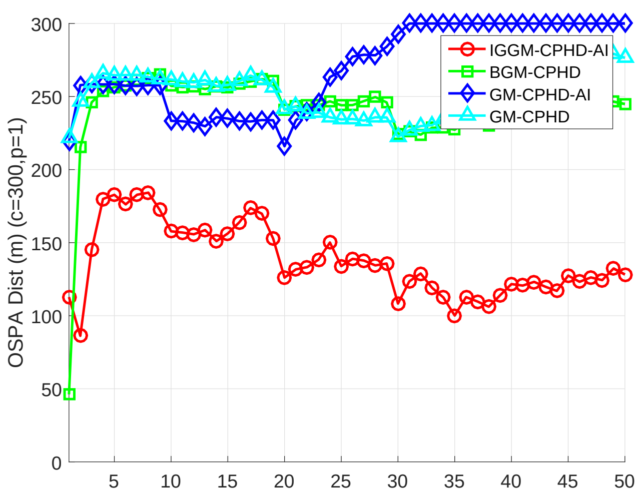

Figure 7: OSPA miss distance versus time for GM-CPHD, GM-CPHD-AI, BGM-CPHD, and IGGM-CPHD-AI filters in strong nonuniform Weibull background (S_5).

and by combining these models with the Gaussian mixture implementation for the PHD, CPHD, and the CBMeMBer filters, we proposed a number of novel filters capturing the AI, namely IGGM-PHD-AI, IGGM-CPHD-AI, and IGGM-CBMeMBer-AI filters. Using an evaluation involving a number of simulation studies, reflecting a suite of realistic problems, we have demonstrated that the proposed filters with AI can simply outperform their counterparts which lack the AI. These results are encouraging and show that multi-object Bayesian filters with AI can help in improving the tracking performance in clutter backgrounds. In fact, embedding AI helps in relaxing a number of assumptions about the spatial uniformity of the clutter or their amplitude distribution being Rayleigh-distributed. In the future, we will apply the proposed method to the multi-object trackers, such as the generalized labeled multi-Bernoulli (GLMB) filter [42, 43] and the labeled multi-Bernoulli (LMB) filter [44], which can estimate object trajectories and their labels, and evaluate the labeling errors [45] of the multi-object trackers with AI in clutter background.

Acknowledgment

This work was supported in part by the National Natural Science Foundation of China (Grant 61671035 and 61501012) and China Scholarship Council.

References

[1] D. Lerro, Y. Bar-Shalom, Automated tracking with target amplitude information, in: 1990 American Control Conference, 1990, pp. 2875–2880.

[2] G. van Keuk, Multihypothesis tracking using incoherent signal-strength information, IEEE Transactions on Aerospace and Electronic Systems 32 (3) (1996) 1164–1170. doi:10.1109/7.532278.

[3] J. McAnanama, T. Kirubarajan, A multiple hypothesis tracker with interacting feature extraction, Signal Processing 92 (12) (2012) 2962 – 2974. doi:https://doi.org/10.1016/j.sigpro.2012.05.030.

[4] L. M. Ehrman, W. D. Blair, Comparison of methods for using target amplitude to improve measurement-to-track association in multi-target tracking, in: 2006 9th International Conference on Information Fusion, 2006, pp. 1–8. doi:10.1109/ICIF.2006.301780.

[5] D. Clark, B. Ristic, B.-N. Vo, B.-T. Vo, Bayesian multi-object filtering with amplitude feature likelihood for unknown object SNR, IEEE Transactions on Signal Processing 58 (1) (2010) 26–37. doi:10.1109/TSP.2009.2030640.

[6] Y. Feng, Z. Wanying, L. Yan, S. Yazhe, Y. Xuanzheng, Cardinality balanced multi-target multi-Bernoulli filter for target tracking with amplitude information, in: 2016 19th International Conference on Information Fusion (FUSION), 2016, pp. 958–964.

[7] Multi-target tracking based on multi-Bernoulli filter with amplitude for unknown clutter rate, MDPI Sensors 15 (2015) 30385–30402. doi:10.3390/s151229804.

[8] M. Mertens, M. Ulmke, Ground moving target tracking using signal strength measurements with the GM-CPHD filter, in: 2012 Workshop on Sensor Data Fusion: Trends, Solutions, Applications (SDF), 2012, pp. 37–42. doi:10.1109/SDF.2012.6327905.

[9] M. Mertens, M. Ulmke, Ground target tracking with RCS estimation utilizing probability hypothesis density filters, in: Proceedings of the 16th International Conference on Information Fusion, 2013, pp. 2145–2152.

[10] M. Mertens, M. Ulmke, W. Koch, Ground target tracking with RCS estimation based on signal strength measurements, IEEE Transactions on Aerospace and Electronic Systems 52 (1) (2016) 205–220. doi:10.1109/TAES.2015.140866.

[11] X. R. Li, N. Li, Integrated real-time estimation of clutter density for track-

ing, IEEE Transactions on Signal Processing 48 (10) (2000) 2797–2804. doi:10.1109/78.869029.

[12] R. L. Streit, L. D. Stone, Bayes derivation of multitarget intensity filters, in: 2008 11th International Conference on Information Fusion, 2008, pp. 1–8.

[13] M. Schikora, W. Koch, R. L. Streit, D. Cremers, Sequential monte carlo method for the ifilter, in: 14th International Conference on Information Fusion, 2011, pp. 1–8.

[14] R. Mahler, A. EI-Fallah, CPHD and PHD filters for unknown backgrounds, III: tractable multitarget filtering in dynamic clutter, in: Proc.SPIE, Vol. 7698, 2010. doi:10.1117/12.849470.

[15] R. Mahler, B.-T. Vo, An improved CPHD filter for unknown backgrounds, in: Proc.SPIE, Vol. 9091, 2014. doi:10.1117/12.2050013.

[16] C. Xin, R. Tharmarasa, M. Pelletier, T. Kirubarajan, Integrated clutter estimation and target tracking using Poisson point process, IEEE Transactions on Aerospace and Electronic Systems 48 (2) (2012) 1210–1234. doi:10.1109/TAES.2012.6178058.

[17] R. Mahler, Advances in Statistical Multisource-Multitarget Information Fusion:, Electronic Warfare, Artech House, 2014.

[18] B.-T. Vo, B.-N. Vo, R. Hoseinnezhad, R. Mahler, Robust multi-Bernoulli filtering, IEEE Journal on Selected Topics in Signal Processing 7 (3) (2013) 399–409. doi:10.1109/JSTSP.2013.2252325.

[19] D. Y. Kim, M. Jeon, Robust multi-Bernoulli filtering for visual tracking, in: The 2014 International Conference on Control, Automation and Information Sciences (ICCAIS 2014), 2014, pp. 47–51. doi:10.1109/ICCAIS.2014.7020566.

[20] A. K. Gostar, R. Hoseinnezhad, A. Bab-Hadiashar, Robust multi-Bernoulli sensor selection for multi-target tracking in sensor networks, IEEE Signal Processing Letters 20 (12) (2013) 1167–1170. doi:10.1109/LSP.2013.2283735.

[21] A. K. Gostar, R. Hoseinnezhad, A. Bab-Hadiashar, Multi-Bernoulli sensor-selection for multi-target tracking with unknown clutter and detection profiles, Signal Processing 119 (Supplement C) (2016) 28 – 42. doi:https://doi.org/10.1016/j.sigpro.2015.07.007.

[22] R. Mahler, Multitarget Bayes filter via first-order multitarget moments, IEEE Transactions on Aerospace and Electronic Systems 39 (4) (2003) 1152–1178. doi:10.1109/TAES.2003.1261119.

[23] B.-T. Vo, B.-N. Vo, A. Cantoni, Analytic implementations of the cardinalized probability hypothesis density filter, IEEE Transactions on Signal Processing 55 (7) (2007) 3553–3567. doi:10.1109/TSP.2007.894241.

[24] B.-T. Vo, B.-N. Vo, A. Cantoni, The cardinality balanced multi-target multi-Bernoulli filter and its implementations, IEEE Transactions on Signal Processing 57 (2) (2009) 409–423. doi:10.1109/TSP.2008.2007924.

[25] R. Mahler, PHD filters of higher order in target number, IEEE Transactions on Aerospace and Electronic Systems 43 (4) (2007) 1523–1543. doi:10.1109/TAES.2007.4441756.

[26] I. J. Cox, S. L. Hingorani, An efficient implementation of Reid's multiple hypothesis tracking algorithm and its evaluation for the purpose of visual tracking, IEEE Transactions on Pattern Analysis and Machine Intelligence 18 (2) (1996) 138–150. doi:10.1109/34.481539.

[27] S. Duffner, J. M. Odobez, Track creation and deletion framework for long-term online multiface tracking, IEEE Transactions on Image Processing 22 (1) (2013) 272–285. doi:10.1109/TIP.2012.2210238.

[28] R. Hoseinnezhad, B.-N. Vo, B.-T. Vo, Visual tracking in background subtracted image sequences via multi-Bernoulli filtering, IEEE Transactions on Signal Processing 61 (2) (2013) 392–397. doi:10.1109/TSP.2012.2222389.

[29] D. Clark, I. T. Ruiz, Y. Petillot, J. Bell, Particle PHD filter multiple target tracking in sonar image, IEEE Transactions on Aerospace and Electronic Systems 43 (1) (2007) 409–416. doi:10.1109/TAES.2007.357143.

[30] R. Mahler, A comparison of clutter-agnostic PHD filters, in: Proc.SPIE, Vol. 8392, 2012. doi:10.1117/12.920799.

[31] M. A. Richards, J. A. Scheer, W. A. Holm, Principles of Modern Radar: Volume I-Basic Principles, SciTech Publishing, 2013.

[32] R. Mahler, Statistical Multisource-Multitarget Information Fusion, Artech House information warfare library, Artech House, 2007.

[33] D. Clark, B. Ristic, B. N. Vo, PHD filtering with target amplitude feature, in: 2008 11th International Conference on Information Fusion, 2008, pp. 1–7.

[34] K. Punithakumar, T. Kirubarajan, A. Sinha, A sequential Monte Carlo probability hypothesis density algorithm for multitarget track-before-detect, in: SPIE Signal and Data Processing of Small Targets 2005, Vol. 5913, 2005, pp. 587–594. doi:10.1117/12.618438.

[35] J. B. Billingsley, A. Farina, M. V. G. F. Gini, L. Verrazzani, Statistical analyses of measured radar ground clutter data, IEEE Transactions on Aerospace and Electronic Systems 35 (2) (1999) 579–593. doi:10.1109/7.766939.

[36] D. C. Schleher, Radar detection in Weibull clutter, IEEE Transactions on Aerospace and Electronic Systems 12 (1976) 736–743. doi:10.1109/TAES.1976.308352.

[37] K. Granström, U. Orguner, Estimation and maintenance of measurement rates for multiple extended target tracking, in: 2012 15th International Conference on Information Fusion, 2012, pp. 2170–2176.

[38] B.-N. Vo, W. Ma, The Gaussian mixture probability hypothesis density filter, IEEE Transactions on Signal Processing 54 (11) (2006) 4091–4104. doi:10.1109/TSP.2006.881190.

[39] Mixture reduction algorithms for target tracking in clutter, in: SPIE Signal and Data Processing of Small Targets 1990, Vol. 1305, 1990, pp. 434–445. doi:10.1117/12.21610.

[40] R. Mahler, B.-T. Vo, B.-N. Vo, CPHD filtering with unknown clutter rate and detection profile, IEEE Transactions on Signal Processing 59 (8) (2016) 3497–3513. doi:10.1109/TSP.2011.2128316.

[41] D. Schuhmacher, B.-T. Vo, B.-N. Vo, A consistent metric for performance evaluation of multi-object filters, IEEE Transactions on Signal Processing 56 (8) (2008) 3447–3457. doi:10.1109/TSP.2008.920469.

[42] B.-T. Vo, B.-N. Vo, labeled random finite sets and multi-object conjugate priors, IEEE Transactions on Signal Processing 61 (13) (2013) 3460–3475. doi:10.1109/TSP.2013.2259822.

[43] B.-N. Vo, B.-T. Vo, D. Phung, labeled random finite sets and the Bayes multi-target tracking filter, IEEE Transactions on Signal Processing 62 (24) (2014) 6554–6567. doi:10.1109/TSP.2014.2364014.

[44] S. Reuter, B.-T. Vo, B.-N. Vo, K. Dietmayer, The labeled multi-Bernoulli filter, IEEE Transactions on Signal Processing 62 (12) (2014) 3246–3260. doi:10.1109/TSP.2014.2323064.

[45] B. Ristic, B.-N. Vo, D. Clark, B.-T. Vo, A metric for performance evaluation of multi-target tracking algorithms, IEEE Transactions on Signal Processing 59 (7) (2011) 3452–3457. doi:10.1109/TSP.2011.2140111.

Appendix A. CBMeMBer filter with AI (CBMeMBer-AI)

For the purpose of extending the CBMeMBer filter with AI, especially when the cardinality distribution of the clutter and the entire clutter PHD are unknown, consider a multi-Bernoulli RFS defined as

$$\ddot{\Pi}_{k|k} = \left\{ \ddot{r}^i_{k|k}, p^i_{k|k}(x^t), q^i_{k|k}(x^c) \right\}_{i=1}^{\ddot{\nu}_{k|k}} \tag{A.1}$$

where, in each Bernoulli RFS, $\ddot{r}^i_{k|k}$ is the existence probability, $p^i_{k|k}(x^t)$ is the target state probability density and $q^i_{k|k}(x^c)$ is the clutter state probability density.

The time-updated multi-Bernoulli RFS can then be expressed as

$$\begin{aligned} \ddot{\Pi}_{k+1|k} &= \ddot{\Pi}^{persist}_{k+1|k} \cup \ddot{\Pi}^{birth}_{k+1|k} \\ &= \left\{ \ddot{r}^i_P, p^i_P(x^t), q^i_P(x^c) \right\}_{i=1}^{\ddot{\nu}_{k|k}} \cup \left\{ \ddot{r}^i_B, p^i_B(x^t), q^i_B(x^c) \right\}_{i=1}^{\ddot{b}_{k+1}} \\ &= \left\{ \ddot{r}^i_{k+1|k}, p^i_{k+1|k}(x^t), q^i_{k+1|k}(x^c) \right\}_{i=1}^{\ddot{\nu}_{k+1|k}} \end{aligned} \tag{A.2}$$

where $\ddot{\nu}_{k+1|k} = \ddot{\nu}_{k|k} + \ddot{b}_{k+1}$ and the components of the persisting multi-Bernoulli RFS are given by [32, 17, 7, 6]

$$\ddot{r}^i_P = \ddot{r}^i_{k|k} \cdot \left(\left\langle p^i_{k|k}, p^t_S \right\rangle + \left\langle q^i_{k|k}, p^c_S \right\rangle \right) \tag{A.3}$$

$$p^i_P(x^t) = \frac{\left\langle p^i_{k|k}, p^t_S \cdot f^t_{k+1|k}(x^t|\cdot) \right\rangle}{\left\langle p^i_{k|k}, p^t_S \right\rangle + \left\langle q^i_{k|k}, p^c_S \right\rangle} \tag{A.4}$$

$$q^i_P(x^c) = \frac{\left\langle q^i_{k|k}, p^c_S \cdot f^c_{k+1|k}(x^c|\cdot) \right\rangle}{\left\langle p^i_{k|k}, p^t_S \right\rangle + \left\langle q^i_{k|k}, p^c_S \right\rangle} \tag{A.5}$$

The observation-updated multi-Bernoulli RFS has the form [32, 17, 7, 6]

$$\begin{aligned}
\ddot{\Pi}_{k+1|k+1} &= \ddot{\Pi}^{\text{legacy}}_{k+1|k+1} \cup \ddot{\Pi}^{\text{update}}_{k+1|k+1} \\
&= \left\{\ddot{r}^i_L, p^i_L(x^t), q^i_L(x^c)\right\}_{i=1}^{\ddot{\nu}_{k+1|k}} \cup \left\{\ddot{r}^j_U, p^j_U(x^t), q^j_U(x^c)\right\}_{j=1}^{\ddot{m}_{k+1}} \\
&= \left\{\ddot{r}^i_{k+1|k+1}, p^i_{k+1|k+1}(x^t), q^i_{k+1|k+1}(x^c)\right\}_{i=1}^{\ddot{\nu}_{k+1|k+1}}
\end{aligned} \tag{A.6}$$

where $\ddot{\nu}_{k+1|k+1} = \ddot{\nu}_{k+1|k} + \ddot{m}_{k+1}$ and the components of the legacy multi-Bernoulli RFS are given by [32, 17, 7, 6]

$$\ddot{r}^i_L = \frac{\ddot{r}^i_{k+1|k} \cdot \left(1 - \left\langle p^i_{k+1|k}, p^\tau_D \right\rangle - \left\langle q^i_{k+1|k}, p^\tau_{FA} \right\rangle\right)}{1 - \ddot{r}^i_{k+1|k} \cdot \left(\left\langle p^i_{k+1|k}, p^\tau_D \right\rangle + \left\langle q^i_{k+1|k}, p^\tau_{FA} \right\rangle\right)} \tag{A.7}$$

$$p^i_L(x^t) = \frac{p^i_{k+1|k} \cdot (1 - p^\tau_D(\sigma^t)))}{1 - \left(\left\langle p^i_{k+1|k}, p^\tau_D \right\rangle + \left\langle q^i_{k+1|k}, p^\tau_{FA} \right\rangle\right)} \tag{A.8}$$

$$q^i_L(x^c) = \frac{q^i_{k+1|k} \cdot (1 - p^\tau_{FA}(\sigma^c)))}{1 - \left(\left\langle p^i_{k+1|k}, p^\tau_D \right\rangle + \left\langle q^i_{k+1|k}, p^\tau_{FA} \right\rangle\right)} \tag{A.9}$$

The components of the updated multi-Bernoulli RFS are given by [32, 17, 7, 6]

$$\ddot{r}^j_U = \frac{\sum_{i=1}^{\ddot{\nu}_{k+1|k}} \frac{\ddot{r}^i_{k+1|k}(1-\ddot{r}^i_{k+1|k})\cdot\eta^j_1}{\left(1-\ddot{r}^i_{k+1|k}\cdot\eta_2\right)^2}}{\sum_{i=1}^{\ddot{\nu}_{k+1|k}} \frac{\ddot{r}^i_{k+1|k}\cdot\eta^j_1}{1-\ddot{r}^i_{k+1|k}\cdot\eta_2}} \tag{A.10}$$

$$p^j_U(x^t) = \frac{\sum_{i=1}^{\ddot{\nu}_{k+1|k}} \frac{\ddot{r}^i_{k+1|k}}{1-\ddot{r}^i_{k+1|k}}\eta^j_3(x^t)}{\sum_{i=1}^{\ddot{\nu}_{k+1|k}} \frac{\ddot{r}^i_{k+1|k}}{1-\ddot{r}^i_{k+1|k}} \cdot \eta^j_1} \tag{A.11}$$

$$q^j_U(x^c) = \frac{\sum_{i=1}^{\ddot{\nu}_{k+1|k}} \frac{\ddot{r}^i_{k+1|k}}{1-\ddot{r}^i_{k+1|k}}\eta^j_4(x^c)}{\sum_{i=1}^{\ddot{\nu}_{k+1|k}} \frac{\ddot{r}^i_{k+1|k}}{1-\ddot{r}^i_{k+1|k}} \cdot \eta^j_1} \tag{A.12}$$

where

$$\eta_1^j = \left\langle p_{k+1|k}, p_D^\tau g_a^{\tau,t}(a_j|\cdot) g_{\tilde{z}}^t(\tilde{z}_j|*) \right\rangle + \left\langle q_{k+1|k}, p_{FA}^\tau g_a^{\tau,c}(a_j|\cdot) g_{\tilde{z}}^c(\tilde{z}_j|*) \right\rangle$$

$$\eta_2 = \left(\left\langle p_{k+1|k}, p_D^\tau \right\rangle + \left\langle q_{k+1|k}, p_{FA}^\tau \right\rangle \right)$$

$$\eta_3^j(x^t) = p_{k+1|k}^i(x^t) \cdot p_D^\tau(\sigma^t) g_a^{\tau,t}(a_j|\sigma^t) g_{\tilde{z}}^t(\tilde{z}_j|\tilde{x}^t)$$

and

$$\eta_4^j(x^c) = q_{k+1|k}^i(x^c) \cdot p_{FA}^\tau(\sigma^c) g_a^{\tau,c}(a_j|\sigma^c) g_{\tilde{z}}^c(\tilde{z}_j|\tilde{x}^c)$$

Appendix B. The IGGM-CBMeMBer-AI Filter

The following assumption is made about the IGGM implementation of the CBMeMBer-AI filter.

Assumption 8. *The current estimated parameters $p_{k|k}$ and $q_{k|k}$ in Multi-Bernoulli RFS are an unnormalized mixture of IGG distributions. That is,*

$$p_{k|k}(x_k^t) \approx \sum_{j=1}^{J_{k|k}^t} \omega_{k|k}^{t,(j)} \mathcal{IGG}(x_k^t; \xi_{k|k}^{t,(j)}) \tag{B.1}$$

$$q_{k|k}(x_k^c) \approx \sum_{j=1}^{J_{k|k}^c} \omega_{k|k}^{c,(j)} \mathcal{IGG}(x_k^c; \xi_{k|k}^{c,(j)}) \tag{B.2}$$

The multi-Bernoulli RFS can also be represented by the set of parameters

$$\left\{ \ddot{r}_{k|k}^i, \left\{ \omega_{k|k}^{t,(i,j)}, \xi_{k|k}^{t,(i,j)} \right\}_{j=1}^{J_{k|k}^t}, \left\{ \omega_{k|k}^{c,(i,j)}, \xi_{k|k}^{c,(i,j)} \right\}_{j=1}^{J_{k|k}^c} \right\}_{i=1}^{\ddot{\nu}_{k|k}}$$

Thus, the time-updated parameters of the Multi-Bernoulli RFS are given by

$$\ddot{r}^{i}_{k+1|k} = \ddot{r}^{i}_{k|k} \cdot \left(p^{t}_{S} \sum_{j=1}^{J^{t}_{k|k}} \omega^{t,(i,j)}_{k|k} + p^{c}_{S} \sum_{j=1}^{J^{c}_{k|k}} \omega^{c,(i,j)}_{k|k} \right) \tag{B.3}$$

$$\omega^{t,(i,j)}_{k+1|k} = \frac{p^{t}_{S} \omega^{t,(i,j)}_{k+1|k}}{p^{t}_{S} \sum\limits_{j=1}^{J^{t}_{k|k}} \omega^{t,(i,j)}_{k|k} + p^{c}_{S} \sum\limits_{j=1}^{J^{c}_{k|k}} \omega^{c,(i,j)}_{k|k}} \tag{B.4}$$

$$\omega^{t,(i,j)}_{k+1|k} = \frac{p^{t}_{S} \omega^{t,(i,j)}_{k+1|k}}{p^{t}_{S} \sum\limits_{j=1}^{J^{t}_{k|k}} \omega^{t,(i,j)}_{k|k} + p^{c}_{S} \sum\limits_{j=1}^{J^{c}_{k|k}} \omega^{c,(i,j)}_{k|k}} \tag{B.5}$$

With the definitions of

$$S^{t,(i)}_{\omega} = \sum_{j=1}^{J^{t}_{k+1|k}} \omega^{t,(i,j)}_{k+1|k} p^{\tau}_{D}$$

and

$$S^{c,(i)}_{\omega} = \sum_{j=1}^{J^{c}_{k+1|k}} \omega^{c,(i,j)}_{k+1|k} p^{\tau}_{FA}$$

The parameters of the legacy multi-Bernoulli RFS are given by

$$\ddot{r}^{L,i}_{k+1|k+1} = \frac{\ddot{r}^{i}_{k+1|k} \cdot \left(1 - S^{t,(i)}_{\omega} - S^{c,(i)}_{\omega}\right)}{1 - \ddot{r}^{i}_{k+1|k} \cdot \left(S^{t,(i)}_{\omega} + S^{c,(i)}_{\omega}\right)} \tag{B.6}$$

$$\omega^{L,t,(i,j)}_{k+1|k+1} = \frac{\omega^{t,(i,j)}_{k+1|k} \cdot (1 - p^{\tau}_{D})}{1 - \left(S^{t,(i)}_{\omega} + S^{c,(i)}_{\omega}\right)} \tag{B.7}$$

$$\omega^{L,c,(i,j)}_{k+1|k+1} = \frac{\omega^{c,(i,j)}_{k+1|k} \cdot (1 - p^{\tau}_{FA})}{1 - \left(S^{t,(i)}_{\omega} + S^{c,(i)}_{\omega}\right)} \tag{B.8}$$

With the definitions of

$$T_{\omega}^{t,(m,i)} = \sum_{j=1}^{J_{k+1|k}^{t}} \omega_{k+1|k}^{t,(i,j)} \cdot p_{D}^{\tau} \cdot \mathcal{L}^{t}(z_{k+1}^{(m)}; \xi_{k+1|k}^{t,(i,j)}, n)$$

and

$$T_{\omega}^{c,(m,i)} = \sum_{j=1}^{J_{k+1|k}^{c}} \omega_{k+1|k}^{c,(i,j)} \cdot p_{FA}^{\tau} \cdot \mathcal{L}^{c}(z_{k+1}^{(m)}; \xi_{k+1|k}^{c,(i,j)}, b)$$

The parameters of the updated multi-Bernoulli RFS are given by

$$\ddot{r}_{k+1|k+1}^{U,(m)} = \frac{\sum_{i=1}^{\ddot{\nu}_{k+1|k}} \frac{\ddot{r}_{k+1|k}^{i}(1-\ddot{r}_{k+1|k}^{i})\cdot\left(T_{\omega}^{t,(m,i)}+T_{\omega}^{c,(m,i)}\right)}{\left(1-\ddot{r}_{k+1|k}^{i}\cdot\left(S_{\omega}^{t,(i)}+S_{\omega}^{t,(i)}\right)\right)^{2}}}{\sum_{i=1}^{\ddot{\nu}_{k+1|k}} \frac{\ddot{r}_{k+1|k}^{i}\cdot\left(T_{\omega}^{t,(m,i)}+T_{\omega}^{c,(m,i)}\right)}{1-\ddot{r}_{k+1|k}^{i}\cdot\left(S_{\omega}^{t,(i)}+S_{\omega}^{t,(i)}\right)}} \tag{B.9}$$

$$\omega_{k+1|k+1}^{U,t,(m,j)} = \frac{\sum_{i=1}^{\ddot{\nu}_{k+1|k}} \frac{\ddot{r}_{k+1|k}^{i}}{1-\ddot{r}_{k+1|k}^{i}} \omega_{k+1|k}^{t,(i,j)} \cdot p_{D}^{\tau} \cdot \mathcal{L}^{t}(z_{k+1}^{(m)}; \xi_{k+1|k}^{t,(i,j)}, n)}{\sum_{i=1}^{\ddot{\nu}_{k+1|k}} \frac{\ddot{r}_{k+1|k}^{i}}{1-\ddot{r}_{k+1|k}^{i}} \cdot \left(T_{\omega}^{t,(m,i)} + T_{\omega}^{c,(m,i)}\right)} \tag{B.10}$$

$$\omega_{k+1|k+1}^{U,c,(m,j)} = \frac{\sum_{i=1}^{\ddot{\nu}_{k+1|k}} \frac{\ddot{r}_{k+1|k}^{i}}{1-\ddot{r}_{k+1|k}^{i}} \omega_{k+1|k}^{c,(i,j)} \cdot p_{FA}^{\tau} \cdot \mathcal{L}^{c}(z_{k+1}^{(m)}; \xi_{k+1|k}^{c,(i,j)}, b)}{\sum_{i=1}^{\ddot{\nu}_{k+1|k}} \frac{\ddot{r}_{k+1|k}^{i}}{1-\ddot{r}_{k+1|k}^{i}} \cdot \left(T_{\omega}^{t,(m,i)} + T_{\omega}^{c,(m,i)}\right)} \tag{B.11}$$